Shear Bands in Monolithic Metallic Glasses: Experiment, Theory, and Modeling

René Hubek[1], Sven Hilke[1], Farnaz A. Davani[1], Mehrdad Golkia[2], Gaurav P. Shrivastav[2,3], Sergiy V. Divinski[1], Harald Rösner[1], Jürgen Horbach[2]* and Gerhard Wilde[1]

[1] Institute of Materials Physics, University of Münster, Münster, Germany, [2] Institut für Theoretische Physik II - Soft Matter, Heinrich-Heine-Universität Düsseldorf, Universitätsstraße 1, Düsseldorf, Germany, [3] Institute for Theoretical Physics, TU Wien, Wien, Austria

For applications, metallic glasses need to retain their high strength over enhanced strain ranges. However, many metallic glasses show catastrophic failure, even in or close to the end of the regime that conventionally has been thought to be elastic. Recent observations of irreversible events at low strains shed some doubt on this nomenclature. In fact, these observations indicate that although the macroscopic response indicates elastic behavior, the microscopic processes might at least partially be irreversible and time-dependent. In that respect, shear bands as the result of shear localization and as the cause of shear softening play a decisive role with respect to the performance of metallic glasses under mechanical load. Therefore, in this work, we are aiming at understanding the correlations between glass structure, glass properties and the thermomechanical history of the glass including the shear bands on one hand and the plastic yielding on the other hand. Various attempts have been made to explain or model the response of metallic glasses to externally applied shear stresses. Hypotheses have been put forward concerning the impact of materials parameters or structural aspects that might favor homogeneous plastic flow. Additionally, scenarios have been suggested for the early stages of anelastic and plastic deformation as well as for the transition to localization and shear band formation/activation. In this contribution, we present a focused viewpoint both from theory and modeling as well as an experimental perspective set on the structure and properties of glasses under shear, with a special focus on shear banding. We also discuss the impact of the local structure of glasses (that depend on the synthesis and processing path-way) in terms of their medium range order. The impact of chemical composition (including microalloying effects) on kinetic properties of shear bands and elasto-plastic properties (Poisson's ratio and three-point bending) is evaluated. These aspects have seen relatively sparse coverage, but are of far-reaching consequences concerning the properties of glasses under mechanical stress. Moreover, these aspects can reveal new insight into the underlying dominant mechanisms and, equally important, allow also to infer about the early stages of strain localization and to analyze the impact of structural heterogeneity or processing conditions on plastic yielding.

Keywords: bulk metallic glass, shear band, shear band diffusion, relaxation, deformation, microalloying

1. INTRODUCTION

Bulk metallic glasses (BMGs), being the youngest member of the materials group of glasses, present a combination of properties that renders them favorable as real-world representatives of model glassy materials with structures and properties that are dominated by local topology and packing fraction (Ashby and Greer, 2006). With respect to mechanical properties and plasticity, as this presents the focus of the present article, metallic glasses as other glasses too show macroscopically homogeneous or inhomogeneous flow, depending on the applied deformation parameters and boundary conditions (i.e., strain rate and temperatures) (Lewandowski et al., 1993; Kumar et al., 2013).

However, upon straining at low homologous temperatures, with the glass transition temperature as a metric, metallic glasses in contrast to covalent glasses, have an extended regime where macroscopic shear stresses are accommodated by localized inhomogeneous flow. Thus, metallic glasses provide conditions that allow to access more easily the investigation of deformation localization than other glassy systems.

Although most glasses, including metallic glasses, do not suffer from low strength and while specifically metallic glasses present a large macroscopically elastic regime, it is still their mechanical performance, which makes them unattractive for applications. In fact, due to the formation of plate-like mesoscopic defects that are termed shear bands, work softening occurs during plastic deformation that leads to catastrophic failure under tension at the latest at the end of the elastic regime. On the other hand, metallic glasses can sustain large macroscopic strain before catastrophic failure if external shear stresses are applied or if the deformation proceeds under (partially) confined conditions. To compare experiment and simulation, it should be noted that the experimental application of an external shear stress, as e.g., during rolling, in almost all cases involves also a significant hydrostatic (pressure) component of the stress tensor.

The commonly accepted picture of plastic deformation of metallic glasses involves structural response on different length and time scales. The initial response involves local yielding of localized regions that involve a group of tens of atoms that undergo a local structural transformation under an applied stress. Such regions that preferentially yield have originally been termed "shear transformation zones" (STZ). Since the early work by Argon (1979) several different terms for related local entities have been coined that describe the local response to an applied shear stress on the basis of a rather similar physical picture. The local shear transformation of a group of atoms then creates a quadrupolar stress field in the adjacent regions, similar to an Eshelby inclusion in an elastic continuum. These stress fields grow, overlap and align upon continuous straining such that percolating shear bands (SB) are formed. In metallic glasses, a broad spectrum of STZs seems to exist (Maaß et al., 2014), which display a rather broad range of activation energies. Some STZs can show rather early activation at low stress within the range that classically has been thought of as reacting purely elastic.

Inherent to this description is the local irreversible response already during macroscopically elastic deformation, due to the broad distribution of activation barriers for the unit shear transformation of a STZ. Thus, strictly speaking glasses have no truly elastic regime, if the microscopic response is taken into account.

Once SBs have formed, deformation proceeds in a localized, inhomogeneous fashion under work softening conditions. Depending on the deformation geometry, the deformation parameters and boundary conditions as well as the specific material, catastrophic failure through fracture will present the final stage of the glass response to the external strain. Even in cases where for a bulk specimen only one major shear band was present and active, slip proceeds often in a stick-slip manner giving rise to the typical "serrated flow" behavior (Klaumünzer et al., 2011). Non-serrated flow behavior can be observed if deformation proceeds at lower temperatures. These observations point toward the importance of relaxation of the glass within the shear bands.

Without regarding specific details or differences between different model descriptions of glass plasticity, it seems clear that the applicability of glasses as structural materials would benefit from enhancing the macroscopic toughness, not necessarily the strength, in order to avoid early failure. For this reason, the response to externally applied stresses needs to be understood from the initial local response of localized groups of atoms to the macroscopic yielding along system-spanning shear bands. In particular, although metallic glasses are rather isotropic, it is necessary to take the atomistic nature of matter into account, since the local STZ activity depends on the local atomic structure and the flow properties of material within the shear band regions are also affected by their atomic structure and the related mechanical properties.

Shear bands have been shown to present a range of values concerning their properties, such as width or specific volume (Klaumünzer et al., 2011; Maaß et al., 2014). Our own work has shown that even for a single shear band, properties such as the specific volume, chemical composition, and atomic configurations may vary along the shear band. In fact, these results indicate unambiguously that both, densification or dilatation occurs, which are probably inherent for stick-slip deformation behavior. Measurements of the atomic diffusion inside shear bands of a metallic glass indicate strongly accelerated diffusion and an intricate dependence on the relaxation of the glass after deformation (Bokeloh et al., 2011). These results render tracer diffusion as a unique and extremely sensitive tool for a detailed investigation of structural changes in shear bands induced by deformation and heat treatment, including the impact of chemical heterogeneity.

Thus, the focus of the present work is on the analysis of the local atomic structures in the glass and on their dependence on strain as well as on the spatio-temporal dynamics of atoms in glasses under strain. Complementing investigations based on experiments and on molecular dynamics simulations have been carried out to elucidate the local response in detail. With this study, we are focusing on generic features of glassy systems and thus provide also a link between metallic and inorganic glasses with respect to their mechanical responses.

2. METHODOLOGY

2.1. Sample Preparation

Experimentally, glassy samples of $Pd_{40}Ni_{40}P_{20}$ (in at.%) were prepared by alloying the appropriate amounts of pure Pd (99.995 wt.% purity) with the compound Ni_2P (99.99 wt.% purity) under partial Argon pressure in an arc melting facility. The resulting crystalline ingot of a few (2–6) grams in weight was repeatedly molten and solidified inside a B_2O_3 flux to extract impurities from the material that are likely to form catalytically potent nucleation sites (Wilde et al., 2000, 2006). Subsequently the metallic alloy was inductively molten inside a SiO_2 crucible that was equipped with a nozzle. At a temperature of about 1,100 K, the melt was blown out through the nozzle by a pressure difference of about 200 mbar of Argon and vitrified inside a massive Cu mold that was kept at room temperature. Estimations concerning the cooling rate during glass synthesis result in about $\left(dT/dt\right)_{eff} \approx 300$ K/s.

The resulting massive samples of glassy $Pd_{40}Ni_{40}P_{20}$ were then checked for the absence of any detectable crystalline fractions. If the absence of detectable crystallinity was confirmed, then the samples were further used for the analysis.

In cases where samples have been annealed, the concept of the limiting fictive temperature according to Tool and Eichlin (1931) has been applied to define the relaxation state on a common basis.

Deformation was applied by cold rolling at room temperature, which amounts to about half of the glass temperature by different means. A macroscopic strain rate of the order of 10^{-1} was utilized to apply a macroscopically uniform deformation on an entire sample. If the quasi-elastic limit was exceeded, then shear bands formed under an angle of about 40–45° with respect to the rolling direction. The total strain was 5–10% measured through the thickness reduction of the plate-like sample.

The amorphous state of each sample was carefully characterized by X-ray diffraction (Siemens D5000) using a Cu cathode, an α-monochromator and a rotating sample holder in the 2θ-geometry. The chemical composition after casting was analyzed by energy dispersive X-ray spectroscopy (EDS) using a Nova Nano SEM 230 (FEI) scanning electron microscope and verified by atomic absorption spectroscopy (Mikroanalytische Labor Pascher, Germany).

Differential scanning calorimetry (DSC) was performed using a Perkin-Elmer Diamond DSC with a typical heating rate of 20 K/min. It was proven that different parts of the same ingots are characterized by almost identical DSC signals verifying the reliability of the data.

Transmission electron microscopy (TEM) was performed using a Titan Themis G3 300 TEM (FEI). Electron-transparent TEM samples were prepared by either electropolishing ($Al_{88}Y_7Fe_5$) or focused ion beam (FIB) preparation (Vit105 and $Pd_{40}Ni_{40}P_{20}$). More details are given in Rösner et al. (2014), Schmidt et al. (2015), and Hieronymus-Schmidt et al. (2017). We used high-angle annular dark-field (HAADF) imaging for the investigations of the shear bands since their visibility is better under these imaging conditions compared to conventional BF/DF imaging. This is because the materials' contrast (Z-contrast) is maximized and the imaging is largely independent of diffraction contrast. For the fluctuation electron microscopy (FEM) analyses, the information was calculated from usually more than 80 individual nanobeam diffraction patterns to have significant good statistics for the variance signal. Sampling with different parallel coherent probe sizes, R, gives insight into the structural ordering length scale and provides a semi-quantitative measure of volume fraction of the medium-range order (peak height or peak integral). This is called VR-FEM (Treacy and Gibson, 1996; Treacy et al., 2005) and was used to extract information on the medium-range order size.

The details of the diffusion measurements are provided in Bokeloh et al. (2011), Binkowski et al. (2016), and Hieronymus-Schmidt et al. (2017). The measurements are performed on macroscopically large samples (typical diameter is about 8 mm) providing sample-averaged concentration–depth profiles over 100 and more microns. The tracer diffusion coefficients are determined using an appropriate solution of the diffusion problem. A typical uncertainty of diffusion measurements is below 50% of the reported diffusion coefficient for the shallow parts of concentration profiles representing fast shear band diffusion. A scatter of the data between the different measurements on identical samples is within these limits.

The Poisson's ratios were determined using ultrasonic measurements carried out in an Olympus 38DL Plus device. A low scatter (several percents at most) has been observed between the data measured on separately cast samples. These deviations were less than the statistical uncertainty (error bars) between multiple measurements on the same sample.

The sample-to-sample variability was found to be low, particularly for the calorimetric, XRD, and ultrasonic measurements. In each case, at least two different samples were analyzed from each cast ingot and a comparison was made for samples produced from different ingots, too. No significant deviations between the measurements were observed.

2.2. Particle-Based Computer Simulation

To model glassforming $Ni_{80}P_{20}$ mixtures under mechanical load, we perform Molecular Dynamics (MD) simulation, i.e., we solve Newton's equations of motion for systems consisting typically of several thousands to about 10^6 particles. The effective interactions between the atoms are described in terms of a Lennard-Jones (LJ) model proposed by Kob and Andersen (1994), where the interaction between a particle of type α and one of type β (α, β = A, B with A = Ni and B = P), separated by a distance r from each other, is given by

$$u_{\alpha\beta}(r) = \phi_{\alpha\beta}(r) - \phi_{\alpha\beta}(r_c) - (r - r_c)\frac{d\phi_{\alpha\beta}}{dr}(r_c), \qquad (1)$$

$$\phi_{\alpha\beta} = 4\varepsilon_{\alpha\beta}\left[\left(\frac{\sigma_{\alpha\beta}}{r}\right)^{12} - \left(\frac{\sigma_{\alpha\beta}}{r}\right)^{6}\right], \text{ for } r \leq r_c \qquad (2)$$

$$= 0, \qquad\qquad\qquad\qquad \text{otherwise.} \qquad (3)$$

The values of the interaction parameters are set to $\varepsilon_{AA} = 1.0$, $\varepsilon_{AB} = 1.5\varepsilon_{AA}$, $\varepsilon_{BB} = 0.5\varepsilon_{AA}$, $\sigma_{AA} = 1.0$, $\sigma_{AB} = 0.8\sigma_{AA}$, and $\sigma_{BB} = 0.88\sigma_{AA}$. In the simulations, the parameters ε_{AA} and σ_{AA} set the units for energy and length, respectively. The other parameters are chosen as $\varepsilon_{AB} = 1.5\varepsilon_{AA}$, $\varepsilon_{BB} = 0.5\varepsilon_{AA}$,

$\sigma_{AB} = 0.8\sigma_{AA}$, and $\sigma_{BB} = 0.88\sigma_{AA}$. The cut-off length for the potentials is $r_c = 2.5\sigma_{AA}$. The masses of both particle species are assumed to be equal, $m = m_A = m_B = 1$. Time is measured in units of $\tau_{LJ} = \sqrt{\frac{m\sigma_{AA}^2}{\varepsilon_{AA}}}$. The equations of motion are integrated with a time step $\delta t = 0.005\,\tau_{LJ}$. Note that in the original model used by Kob and Andersen, the third term on the right-hand side of Equation (1) was not introduced, leading to a discontinuity of the forces at r_c. Moreover, in their model the cut-off lengths for the potentials were set to $r_c^{\alpha\beta} = 2.5\sigma_{\alpha\beta}$, i.e., they used different cut-off lengths for AA, AB, and BB interactions.

To give an idea about the conversion to the experimental length, energy, and time scales, we can convert ε_{AA} and σ_{AA} to typical scales of a Ni-P alloy and set $\varepsilon_{AA} = 1,000\,k_B\,K$ and $\sigma_{AA} = 3.5\,Å$ (with k_B the Boltzmann constant). In these units, the LJ time scale is $\tau_{LJ} = 0.93\,ps$ (here, we have set m to the mass of Ni, $m = 97.431 \times 10^{-27}\,kg$). In the following, we consider systems at the mass density $\rho = 1.2\,m/\sigma_{AA}^3 = 2.73\,g/cm^3$. Systems in a cubic box geometry with a linear size $L = 30\,\sigma_{AA} = 105\,Å$ are considered. These systems contain 32,400 particles.

Typically, the protocol of our simulations is as follows: We equilibrate the system in the supercooled liquid state at a temperature $T = 0.44\,\varepsilon_{AA}/k_B = 440\,K$ over a time scale of $10^4\,\tau_{LJ} \approx 9.3\,ns$. Note that the mode coupling transition temperature for the considered binary LJ mixture is at $T_c = 0.435\,\varepsilon_{AA}/k_B = 435\,K$. Then, we perform a quench from the supercooled liquid to a glass state at $T = 0.2\,\varepsilon_{AA}/k_B = 200\,K$. Here, the sample is annealed for $t_w = 10^4\,\tau_{LJ}$, followed by the shearing of the system with a constant strain rate $\dot{\gamma}$. The shear is realized via Lees-Edwards boundary conditions (Lees and Edwards, 1972), imposing a planar Couette flow along the xz plane in the direction of x. The system's temperature is kept constant via dissipative particle dynamics which provides local momentum conservation and an unbiased thermostating of the system (Soddemann et al., 2003). The LAMMPS package (Plimpton, 1995) is used to perform the simulations. As a typical shear rate, we have chosen $\dot{\gamma} = 10^{-4}/\tau_{LJ} \approx 0.1\,ns^{-1}$. More details about details of the simulation can be found in Binkowski et al. (2016), Shrivastav et al. (2016a), Shrivastav et al. (2016b), and Golkia et al. (2020).

The response to an external shear is well understood for the case of a fluid in the Newtonian or linear response regime (Chhabra and Richardson, 2008), i.e., at sufficiently low shear rates $\dot{\gamma}$. In the steady state, one obtains a homogeneously flowing fluid, associated with a linear velocity profile in the considered planar Couette flow geometry. The steady-state shear stress in the Newtonian regime exhibits a linear dependence on shear rate, $\sigma_{ss} = \eta\dot{\gamma}$ with η the shear viscosity. When one decreases temperature toward the glass transition temperature in a glassforming fluid, the Newtonian regime shifts to smaller and smaller shear rates. Eventually, at the glass transition, the Newtonian regime is no longer accessible experimentally. So, below the glass transition, there is no linear response regime and the flow curve, i.e., σ_{ss} as a function of $\dot{\gamma}$, can be usually well-fitted by a Herschel-Bulkley law at low shear rates (Chhabra and
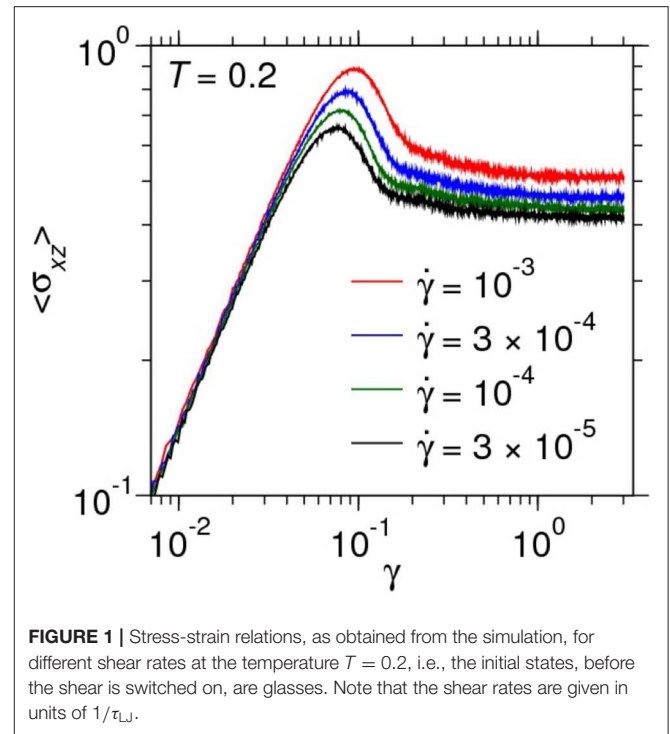
FIGURE 1 | Stress-strain relations, as obtained from the simulation, for different shear rates at the temperature $T = 0.2$, i.e., the initial states, before the shear is switched on, are glasses. Note that the shear rates are given in units of $1/\tau_{LJ}$.

Richardson, 2008; Ovarlez et al., 2013),

$$\sigma_{ss} = \sigma_Y + A\dot{\gamma}^\alpha \qquad (4)$$

with the yield stress σ_Y, an amplitude A, and an exponent α which is usually in the range between 0.4 and 0.6. For a recent discussion of the Herschel-Bulkley law in glasses, we refer to Agoritsas and Martens (2017). It predicts the existence of a yield stress σ_Y which has, however, a purely kinetic origin. It is due to the inaccessibility of the Newtonian regime on the time scale of the experiment or simulation.

Both supercooled liquids in the non-Newtonian regime and glasses typically display a similar behavior with respect to the average shear stress (Zausch et al., 2008; Zausch and Horbach, 2009), $\langle\sigma\rangle$, as a function of the strain $\gamma = \dot{\gamma}t$. In **Figure 1**, stress-strain relations are shown for different shear rates at the temperature $T = 0.2$, i.e., the initial unsheared samples are in a glass state. Note that the results in **Figure 1** are obtained from an average over 250 independent runs for each shear rate. For $\gamma < 0.08$, there is an elastic response to the external shear where the stress increases linearly with increasing γ, $\langle\sigma_{xz}\rangle = G\gamma$ with G the shear modulus. The curves for the different shear rates are almost on top of each other which indicates that the shear modulus G has only a very weak dependence on $\dot{\gamma}$. The elastic regime is followed by a stress overshoot around a strain of the order of 0.1 from where the stress decays toward the steady-state shear stress. A characteristic feature in the latter transient regime is the occurrence of inhomogeneous flow patterns; in particular, there is the possibility of the formation of horizontal shear bands, i.e., bands of high mobility parallel to the flow direction. Although these horizontal bands are transient, they are relatively

long-lived. One observes a sublinear growth of their width as a function of strain (Alix-Williams and Falk, 2018; Golkia et al., 2020). The stress-strain relations of supercooled liquids in the non-Newtonian regime also show typically a maximum around $\gamma \approx 0.1$ and, at sufficiently low shear rates, inhomogeneous flow patterns (Golkia et al., 2020). As in glasses, there are also long-ranged strain correlations in supercooled liquids (Chattoraj and Lemaître, 2013; Hassani et al., 2018), similar to those caused by Eshelby inclusions in an elastic medium. However, horizontal shear bands have not been observed in supercooled liquids under shear (Golkia et al., 2020). Their appearance in simulated glasses under shear is discussed in more detail below.

3. STRUCTURE OF SHEAR BANDS

3.1. Microstructural Investigations Using Analytical Transmission Electron Microscopy (TEM) and Fluctuation Electron Microscopy (FEM)

Our experiments showed an alternation of higher and lower density regions along the propagation direction of the shear bands for three different metallic glasses (Rösner et al., 2014; Schmidt et al., 2015; Hieronymus-Schmidt et al., 2017; Hilke et al., 2019). The density changes along shear bands are correlated with small deflections along the propagation direction (see **Figure 2**), structural changes in the medium-range order (MRO) and in some incidences, with compositional changes. The observation of densification for the bright shear band regions was somewhat unexpected since macroscopic measurements reported dilation only (Lechner et al., 2010; Klaumünzer et al., 2011; Shao et al., 2013).

3.2. New Method Developed

A new method was developed to quantify the density changes using the intensity of the recorded electron micrographs (Rösner et al., 2014). A simple correlation was found for the intensity ratio of shear band and the matrix material (ISB/IM) with the relative density changes ($\Delta\rho/\rho$). Simulations confirmed the high precision of this approach (Radek et al., 2018), $\frac{\Delta\rho}{\rho} = \frac{I_{SB}}{I_M} - 1$.

3.3. Model Based on Continuum Mechanics Explaining the Observations of Density Oscillations With Smaller Positive and Larger Negative Amplitudes as Deformation Mechanism

A model was proposed based on the idea that the density changes in the shear bands are caused by an alignment of quadrupolar stress concentrators (Eshelby-like quadrupoles) (Dasgupta et al., 2012, 2013), which follow a $\propto \cos(4\theta)/r^3$ dependence (Hieronymus-Schmidt et al., 2017). This model provides the non-trivial connections between the different magnitudes for dilated and densified regions (see **Figure 2**) and the bulk modulus K. The difference in magnitude between the negative and positive amplitudes can be explained now since the amplitude height of the density variations scales with

the compressibility $\kappa = 1/K$ of the material, which is the second derivative of the interatomic potential with respect to the volume or the curvature of the interatomic potential. Due to the asymmetry of the interatomic potential it is easier to achieve expansion than compression.

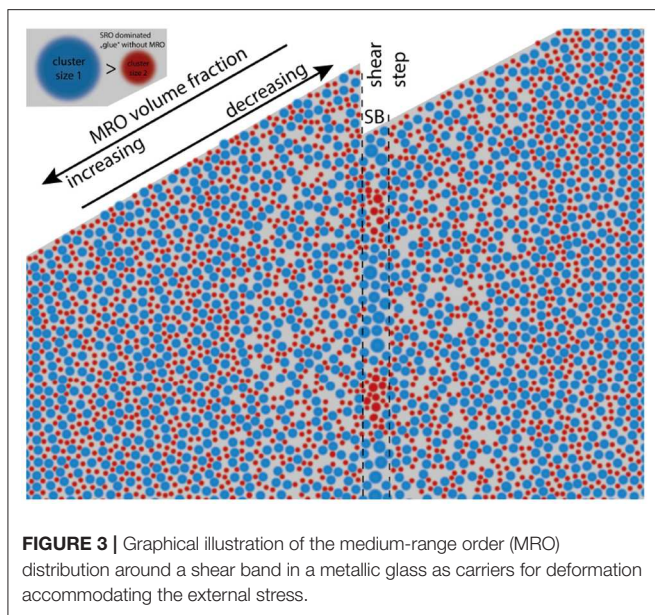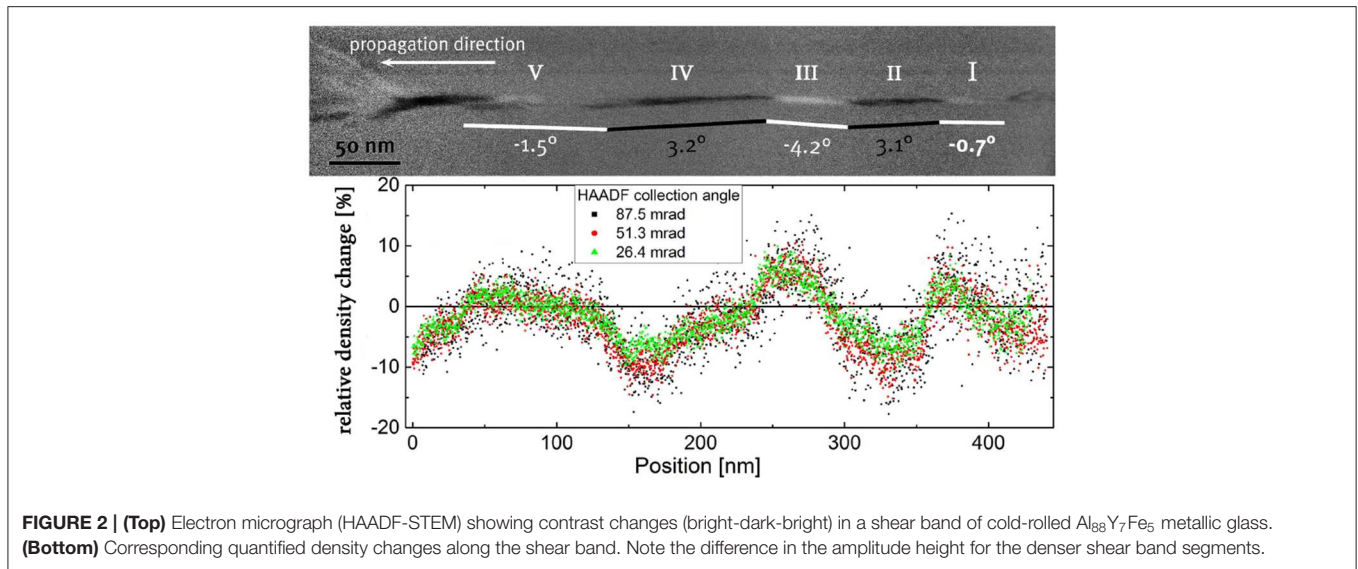## 3.4. Topological Order (MRO) as the Structural Element in Glasses

The medium-range order of different metallic glasses was quantified using fluctuation electron microscopy (FEM) (Treacy and Gibson, 1996; Voyles and Muller, 2002; Treacy et al., 2005). FEM is a microscopic technique that is sensitive to MRO in disordered materials since it contains information about the four-body correlation of atom pairs (pair-pair correlation function). For this purpose, a statistical analysis of the diffracted intensities $I(\vec{k}, R, \vec{r})$ from nanometric volumes obtained either by tilted dark-field TEM or STEM microdiffraction was carried out. Sampling with different parallel coherent probe sizes, R, enhances the sensitivity to the structural ordering length scales and provides a semi-quantitative measure of the MRO volume fraction. This is called variable resolution FEM (VR-FEM).

This technique was applied to our metallic glass materials. The MRO of both as-cast and deformed states of different metallic glass [Al88Y7Fe5, Zr52.5Cu17.9Ni14.6Al10Ti5 (Vitreloy105), $Pd_{40}Ni_{40}P_{20}$ and α-Si] were analyzed using variable resolution fluctuation electron microscopy (VR-FEM). The investigated metallic glasses span the entire range of characteristic properties of metallic glasses [marginal to good glassforming ability (GFA) as well as brittle to ductile behavior]. After deformation we observe significant structural changes in the MRO inside the shear bands and the adjacent matrix; the MRO was altered in terms of types, size and volume fractions (Schmidt et al., 2015; Hilke et al., 2019). The changes in the matrix MRO upon deformation confirm the existence of a shear-affected zone around the shear band. The results are graphically illustrated in **Figure 3**.

The presence of MRO was also confirmed for amorphous Si (α-Si) (Radić et al., 2019), which in turn, span the range from metallic glasses to inorganic silica glasses. In essence, the MRO regions can also be seen as carriers of plasticity (like shear transformation zones) bridging the mechanical behavior of metallic glasses and silica glasses. This concept also suggests connections to the physics of granular materials and jammed systems with the MRO as granules.

4. CHARACTERIZATION OF SHEAR BANDS ON A MICROSCOPIC LEVEL

As we have mentioned above, our non-equilibrium molecular dynamics simulations of the $Ni_{80}P_{20}$ model show the occurrence of horizontal shear bands in the considered sheared glasses at the temperature $T = 0.2\,\varepsilon_{AA}/k_B$ (in real units, this corresponds to a temperature of the order of $200\,K$, see above). Now, we characterize the properties of horizontal shear bands and discuss the conditions under which they form.

FIGURE 2 | (Top) Electron micrograph (HAADF-STEM) showing contrast changes (bright-dark-bright) in a shear band of cold-rolled $Al_{88}Y_7Fe_5$ metallic glass. **(Bottom)** Corresponding quantified density changes along the shear band. Note the difference in the amplitude height for the denser shear band segments.

FIGURE 3 | Graphical illustration of the medium-range order (MRO) distribution around a shear band in a metallic glass as carriers for deformation accommodating the external stress.

Unlike the supercooled liquid state, the response of glasses to shear can be qualitatively different from sample to sample. In the transient regime after the stress overshoot, one can obtain different flow patterns when the shear is applied to glass samples with the same thermal history. This is exemplified in **Figure 4**. Here, **Figures 4a,b** show respectively the shear stress and the potential energy as a function of strain γ for two individual samples. While the stress-strain relations are similar for both samples, the potential energy shows significant differences with respect to the behavior between $\gamma_{max} \approx 0.08$ (location of the stress maximum) and the steady state which is reached for both samples around $\gamma = 1.0$. In one sample (corresponding to the cyan curve in the figure), the potential energy has a shallow minimum after a local maximum at γ_{max}, followed by

an increase toward the steady-state value U_{ss}. The other sample (corresponding to the orange curve), on the contrary, increases monotonically toward U_{ss}. In fact, the two samples are associated with different flow patterns, one with two vertical bands (orange curve) and the other one with a horizontal band (cyan curve). This is illustrated for each case in the snapshots in **Figure 4** at the strains $\gamma = 0.2, 0.5, 1.0,$ and 3.0. These snapshots show mobility color maps of single particle square displacements in z-direction (direction of the shear gradient), $\delta r_z^2(t) = (r_{iz}(t) - r_{iz}(0))^2$ with $r_{iz}(t)$ the z-component of the coordinate of particle i at time t. We can infer from the snapshots that the horizontal shear band (**Figure 4a**) has a longer lifetime than the vertical bands (**Figure 4b**).

An interesting question is about the connection of the type of shear band with structural heterogeneities in the initial quiescent glass sample. Is it predetermined by the initial configuration whether it will evolve into a vertical or a horizontal shear band? To analyze this issue, we have done shear simulations starting from the same sample, but using different initial random seeds for the DPD thermostat. In some cases, horizontal shear bands, albeit at different locations, are formed, while in other cases vertical bands are seen where the evolution toward the homogeneous steady-state flow is significantly faster. This indicates that the type of shear band and also its location is not predetermined by the initial undeformed glass. Note that our findings are in agreement with those of Gendelman et al. (2015) for a two-dimensional binary Lennard-Jones glass model in a confined geometry with circular shape. Their and our results challenge the assumption made in shear transformation zone (STZ) theory (Taub and Spaepen, 1980; Falk and Langer, 1998), according to which plastic events happen at some hot spots that are connected to structural heterogeneities in the glass state from which the shear is started.

The formation of horizontal shear bands becomes more likely with increasing system size (Golkia et al., 2020) and it becomes more pronounced also at very low temperature where the thermal motion of the particles is no longer relevant. Using an athermal
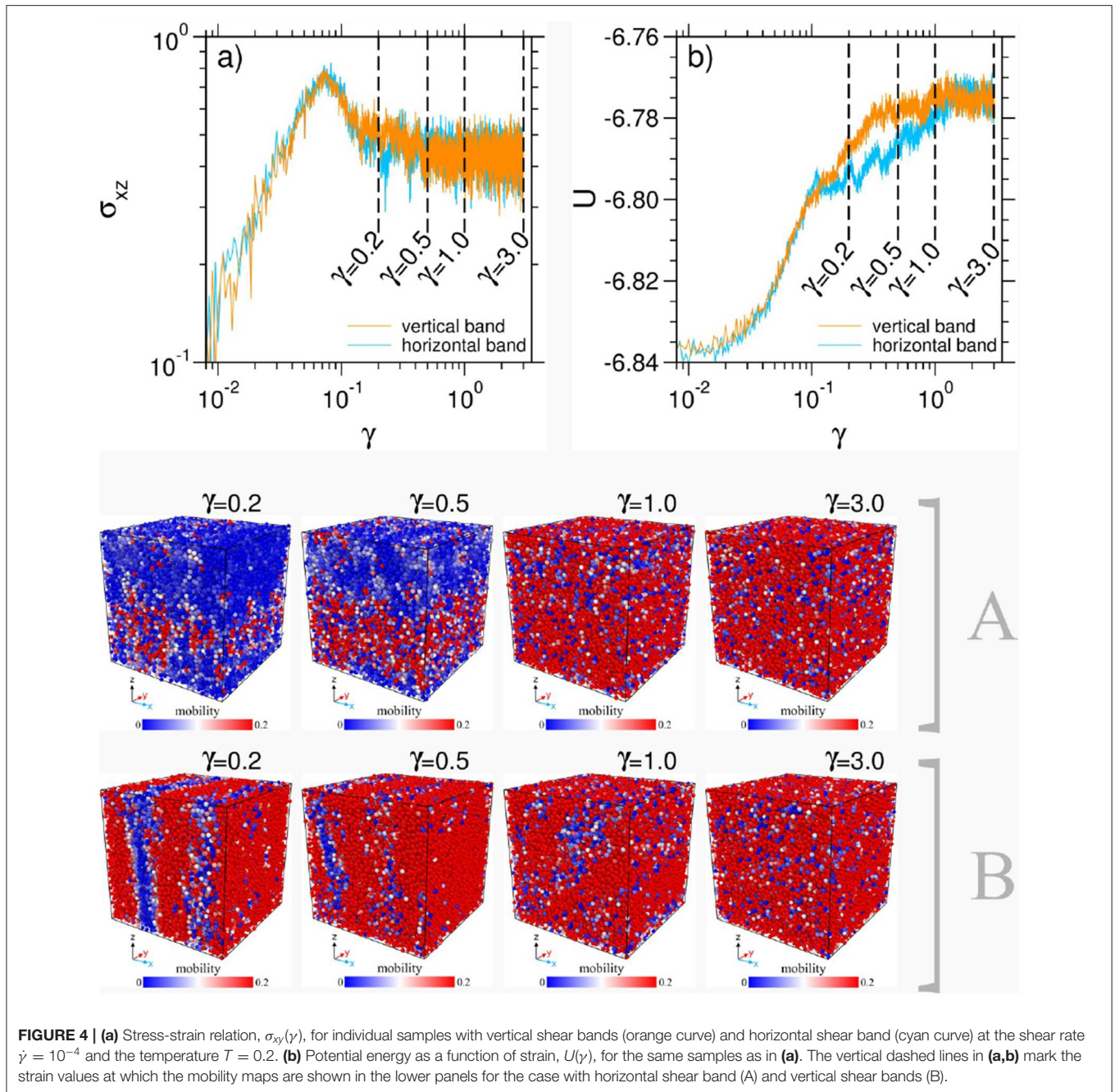
FIGURE 4 | **(a)** Stress-strain relation, $\sigma_{xy}(\gamma)$, for individual samples with vertical shear bands (orange curve) and horizontal shear band (cyan curve) at the shear rate $\dot{\gamma} = 10^{-4}$ and the temperature $T = 0.2$. **(b)** Potential energy as a function of strain, $U(\gamma)$, for the same samples as in **(a)**. The vertical dashed lines in **(a,b)** mark the strain values at which the mobility maps are shown in the lower panels for the case with horizontal shear band (A) and vertical shear bands (B).

quasi-static shear (aqs) protocol, Ozawa et al. (2018) have demonstrated that the formation of a shear band is intimately linked to the degree of annealing of the initially undeformed glass sample. Then, horizontal shear bands are associated with a very sharp stress drop that becomes sharper with increasing system size which is reminiscent of a first-order phase transition. In fact, the authors of Ozawa et al. (2018) argue that, under athermal conditions, the yielding of a well-annealed amorphous solid can be interpreted as a first-order non-equilibrium phase transition. It is also interesting that inhomogeneous states with horizontal shear bands can be stabilized via oscillatory shear. This has been

recently demonstrated in a simulation study by Parmar et al. (2019).

Our work shows that the formation of horizontal shear bands is associated with a peculiar behavior of the system's potential energy. After the formation of such a band right after the occurrence of the stress drop in the stress-strain relation, the potential energy function $U(\gamma)$ has local minimum, followed by an increase of U with further deformation toward the steady state value. We note that this behavior becomes more pronounced with decreasing temperature as well as the degree of annealing of the initial unsheared glass state (Golkia et al., 2020). The findings
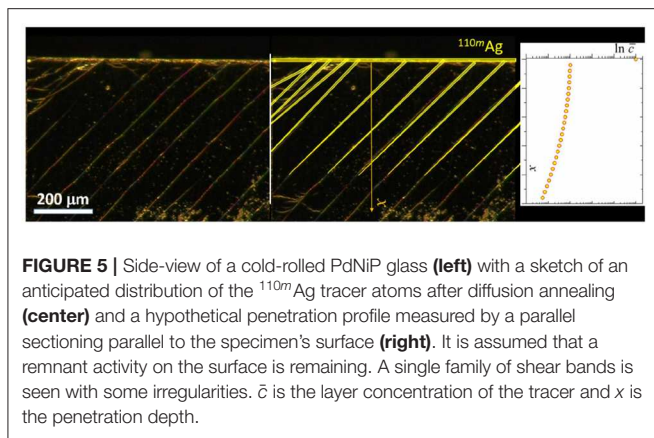
FIGURE 5 | Side-view of a cold-rolled PdNiP glass **(left)** with a sketch of an anticipated distribution of the ^{110m}Ag tracer atoms after diffusion annealing **(center)** and a hypothetical penetration profile measured by a parallel sectioning parallel to the specimen's surface **(right)**. It is assumed that a remnant activity on the surface is remaining. A single family of shear bands is seen with some irregularities. $\bar{c}$ is the layer concentration of the tracer and x is the penetration depth.

may also reveal what one sees on the typical experimental time and length scales which are both much larger than those of the simulation. In experiments of bulk metallic glasses, shear banded structures appear to maintain after yielding and a subsequent switch-off of the mechanical load. This is due to the efficient stress release in combination with the minimization of the system's potential energy via the formation of a shear band.

5. ATOMIC TRANSPORT ALONG SHEAR BANDS

Detailed calorimetric investigations substantiated an absence of any measurable changes of the calorimetric response of a bulk metallic glass, particularly of a model PdNiP one (Mitrofanov et al., 2014, 2015), on shear banding induced by cold rolling to low strain, about 10% of thickness reduction. All main calorimetric parameters, including glass transition temperature, T_g, crystallization temperature, total enthalpy, and low temperature heat capacity remain unchanged in the limits of typical experimental uncertainties (Mitrofanov et al., 2014, 2015).

However, the structure and local atomic configurations—as revealed by, e.g., the MRO parameter (Hilke et al., 2019)—are different in the shear bands from the surrounding matrix. The strain-induced differences in the atomic configurations might be traced by dedicated investigations of the atomic transport rates, and indeed the tracer diffusion measurements substantiated kinetic differences between the shear bands and the glassy matrix (Bokeloh et al., 2011).

5.1. Shear Bands as Short-Circuits for Enhanced Diffusion

In **Figure 5**, a side view on off-sets induced by shear band propagation is presented (left panel). Before the one-pass rolling to about 5%, the sample was polished to a mirror-like finish that allowed to visualize the shear bands.

In a typical radiotracer experiment (Paul et al., 2014), we are depositing a tiny amount of a suitable radioactive isotope on the polished surface and subjecting the specimen to a diffusion annealing treatment. In order to quantify the diffusion rates along the shear bands, the conditions of the diffusion treatment

are typically chosen which corresponds to the absence of any volume diffusion in the glass (i.e., the corresponding diffusion depths, $\sqrt{D_v t}$, are smaller than an interatomic distance, with D_v and t being the volume diffusion coefficient and the diffusion time, respectively). An anticipated tracer distribution after such annealing is sketched in **Figure 5** (central panel). In this figure, one can recognize a remnant activity of the tracer material (in a particular case of the ^{110m}Ag isotope) on the surface, which correspond to not-diffused isotopes and some potential irregularities in the depth distribution of the tracer atoms due to heterogeneities of the shear banding. Formally, these diffusion conditions correspond to the C-type kinetic regime of diffusion along short circuits in crystalline solid after Harrison's classification (Harrison, 1961; Paul et al., 2014).

After diffusion annealing, the sample is sectioned by, e.g., precision mechanical grinding, parallel to the initial surface in thin slices and the *total* activity in the sections is measured. As a result, a penetration profile corresponding to the layer activity of the tracer, $\bar{c}$, vs. the penetration depth, x, is measured, **Figure 5**, right panel.

In some cases, we are applying a second tracer, e.g., the ^{57}Co to the sample surface after annealing just before sectioning. If there would be micro-cracks in the sample, the ^{57}Co isotope would be detectable to similar depths as ^{110m}Ag. Our experiments (Bokeloh et al., 2011) confirmed the absence of the second isotope at large depths and substantiated a deep penetration of the first isotope, which experienced a diffusion annealing treatment. Thus, the observed deep penetration of the ^{110m}Ag isotope is not due to deformation-induced cracks.
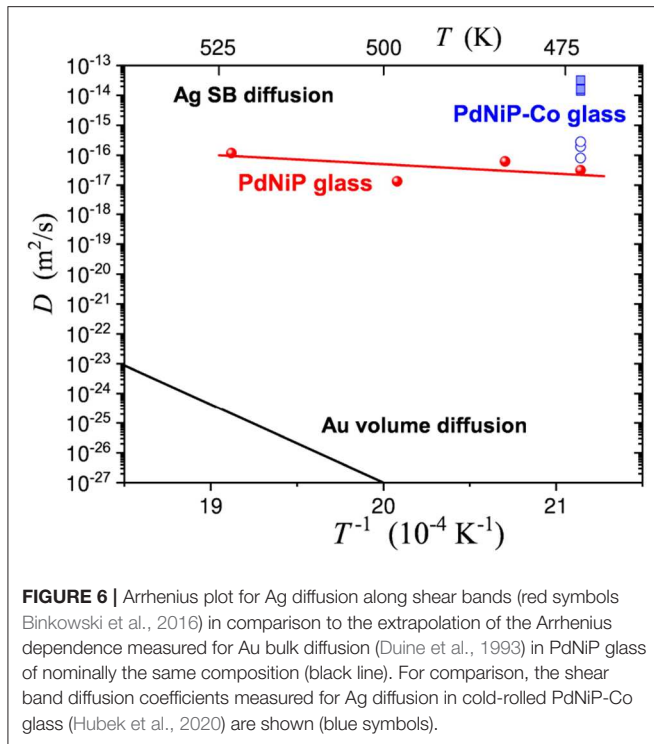
The shear band diffusion coefficients, D_{sb}, can be determined as (Paul et al., 2014)

$$D_{sb} = \frac{q}{4t} \left(-\frac{\partial \ln \bar{c}}{\partial x^2} \right)^{-1}. \tag{5}$$

Here, the factor q takes into account the orientation of the short-circuit path with respect to the normal to the sample surface and it is equal to about 2 since the shear bands are oriented at about 45° to the sample surface.

The determined shear band diffusion coefficients of Ag atoms, D_{sb}, turned out to be eight to nine orders of magnitude larger than the volume diffusion coefficients measured in as-cast PdNiP samples for Au (Duine et al., 1993) or Pd (Bartsch et al., 2010) tracers. At 473 K, the volume diffusion coefficients are less than 10^{-26} m^2/s at 473 K, while the shear band diffusion coefficients are of the order of 10^{-17} m^2/s at the same temperature (**Figure 6**).

These data substantiate the possibility to use tracer diffusion measurements in deformed glasses as a unique and very sensitive probe of changes of local atomic structures. Tracking the shear band diffusion in dependence of the annealing time in the same way as the as-quenched and deformed material indicates differences in structure of the matrix material as well as the shear band structure in the relaxed material.

FIGURE 6 | Arrhenius plot for Ag diffusion along shear bands (red symbols Binkowski et al., 2016) in comparison to the extrapolation of the Arrhenius dependence measured for Au bulk diffusion (Duine et al., 1993) in PdNiP glass of nominally the same composition (black line). For comparison, the shear band diffusion coefficients measured for Ag diffusion in cold-rolled PdNiP-Co glass (Hubek et al., 2020) are shown (blue symbols).

FIGURE 7 | Time dependence of diffusion enhancement in model PdNiP glass deformed by cold-rolling as compared to that in PdNiP preliminary relaxation annealed **(Top)** or to as-quenched Co-microalloyed PdNiP glass **(Bottom)**. Further, the time dependencies of the diffusion coefficients are compared with that of the fictive temperature $T_{fictive}$ of the BMGs. The systematic uncertainty of a single diffusion experiments can be approximated to be about 50%. These are not shown for better visibility of the graph.

5.2. Relaxation Behavior of Enhanced Shear Band Diffusion

The shear band diffusivities behave in an abnormal fashion (unlike expected when structural relaxation is considered to lower diffusivities) for the deformed as-quenched samples. Yet, this behavior is not observed for samples relaxed previously to deformation. In contrast to the deformed as-quenched metallic glass state, the deformed relaxed samples reach much earlier a metastable equilibrium state, in which the atomic mobility inside the shear bands is no longer time dependent.

In cold-rolled as-quenched Co-free PdNiP glass, fast shear band diffusion was measured (the diffusion coefficients are of the order of 10^{-17} m^2/s) and interpreted in terms of a single family of shear bands. A cross-over relaxation behavior of shear band diffusion is observed and explained as a counteraction of redistribution of excess free volume in deformation-modified volume and in shear bands.

Relaxation-annealed PdNiP at 503 K for 1 day reveal unexpectedly the existence of two kinds of short-circuit contributions with conventional fast (about 10^{-17} m^2/s) and ultra-fast diffusion (about 10^{-15} m^2/s) coefficients (**Figure 7**).

The ultra-fast shear band diffusivity in relaxed samples shows not only time-independent, but rather shows unexpectedly a diffusion enhancement in comparison to the deformed as-quenched state of about 1–2 orders of magnitude (**Figure 7**). Since atoms in general need less energy to move through a more open structure, the shear band structure in relaxed glasses differs to the shear bands in as-quenched glasses indicating the presence of an enhanced amount of free volume.
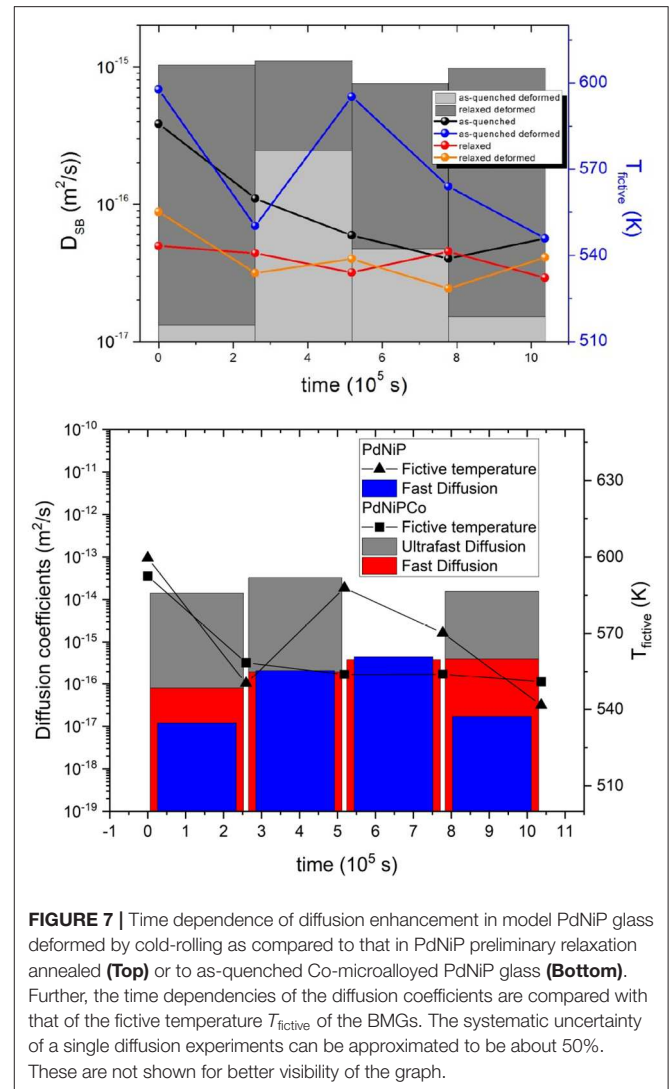
Similarly, the Co micro-alloyed glass reveals unambiguously two families of short circuits, namely the "fast" diffusion paths (essentially the same diffusion coefficients) and a second type of "ultrafast" paths (with diffusion coefficients of the order of 10^{-15}–10^{-14} m^2/s), correspondingly open and filled blue symbols in **Figure 6**. We are attributing this second path to a special type of shear band. Such shear bands are either absent in the as-quenched Co-free glass or their number density is below the detection limit of the applied radiotracer technique. There is a clear difference between the optically observable primary and secondary shear bands—available in fact in both types of the glassy systems—and the kinetically different shear bands. So far, it is a very first observation of this behavior.

Furthermore, the exceptional time-evolution of the glass transition observed in the heat flow curves of the deformed as-quenched glass is not observed for the relaxed and deformed glass. The macroscopically measurable atomic rearrangements during annealing are missing. Annealing treatments below the glass transition temperatures of glasses are known to

change the glassy structure causing physical aging. Free volume annihilates and "anneals out" as the structural relaxation occurs (Haruyama and Inoue, 2006). The more dense structure contains decreasingly sites for increased atomic movement known as STZ. Thus, taking the STZs as precursors for the formation of shear bands, shear band emergence is strongly decreased. The excess energy barrier to effectuate a shear transformation is much higher when lacking of adequate amount of free volume. If the amount of shear deformation is, however, high enough to provide the necessary energy, shear transformations are activated. An increase in input energy engenders an increase in release of energy during shear band formation and, as a resulting consequence, may force a more open structure of the resulting shear bands.

We may argue that shear banding in relaxed glass induces stronger variation of local configurations with respect to those in as-quenched glasses and, importantly, these stronger variations correspond to energy configurations being more stable with respect to their further structural relaxation. As a result, we may suggest that the shear bands induced in relaxed metallic glass represent a more stable, but different glassy configuration as the matrix itself that could be further investigated with respect to production of nano-glasses (Gleiter, 2013) by plastic deformation. These changes are strongly localized at the shear bands and the corresponding contribution is almost invisible in the DSC measurements.

5.3. Micro-Alloying

5.3.1. Structural Changes and Mechanical Response

Micro-alloying was performed on monolithic $Pd_{40}Ni_{40}P_{20}$ bulk metallic glass by adding small amounts of Co and Fe. The material was melted in a melt-spinner using induction melting and subsequently casted into Cu-molds (Nollmann et al., 2016) (see the flow chart of **Figure 8**). The amorphous state was confirmed by X-ray diffraction and it was further characterized by electron diffraction and differential scanning calorimetry, left and central panels in **Figure 8**, respectively. The 3-point bending tests were performed showing an improved ductility when Co was added, **Figure 8**, right panel. However, the addition of Fe led to embrittlement, whereas the ternary $Pd_{40}Ni_{40}P_{20}$ alloy showed quite some ductility. Recent microstructural investigations using fluctuation electron microscopy showed that a second larger MRO correlation length was observed in the ductile material (Davani et al., 2020), which explains the difference in the deformability.

5.3.2. Mechanical Properties (Poisson's Ratio) of Deformed BMGs

It is still a matter of debate, whether the ductility of bulk metallic glasses is related to their elastic constants. Here we present experiments on the Poisson's ratio of Pd-based BMG in dependence of the degree of deformation. For this purpose, $Pd_{40}Ni_{40}P_{20}$ was cold rolled up to 50% deformation and the elastic constants were subsequently determined from ultrasonic measurements (Nollmann et al., 2016). Our experiments (**Figure 9**) show that there is no measurable change in the Poisson's ratio, comparing undeformed with deformed metallic glass.

5.3.3. Shear Band Diffusion in Microalloyed State

The radiotracer measurements substantiated that cold-rolled Co-microalloyed PdNiP glasses reveal the existence of two families of shear bands, slow and fast ones (Hubek et al., 2020), see open and filled blue symbols in **Figure 6**. From the measurements with the ^{57}Co tracer the resulting ratio for the PdNiPCo profiles lies between 1:10 to 1:100 of ultrafast to fast diffusion paths.

Multiple kinds of shear bands, defined as primary and secondary (Schroers and Johnson, 2004; Chen and Lin, 2010) or "hot" and "cold" (Lewandowski and Greer, 2005) shear bands, were previously reported in the literature. While one could interpret the two measured shear band diffusion coefficients as indication for primary and secondary shear bands, this is not clearly the case.

In the present case of a low imposed deformation, mainly primary shear bands were detected (Hubek et al., 2020). However, a strong heterogeneity of shear band offsets was reported (Hubek et al., 2020) for Co-microalloyed PdNiP glass. Those results indicate a correlation between the distribution of shear band offsets and the existence of different families of short-circuit diffusion paths in the PdNiP-based metallic glasses. Although our measurements do not provide a direct verification that the ultra-fast diffusion paths are represented by the shear bands with large shear offsets, there is a direct correlation between the structure heterogeneity and the kinetic heterogeneity of the shear band properties. This finding is encouraging and demands further investigations.
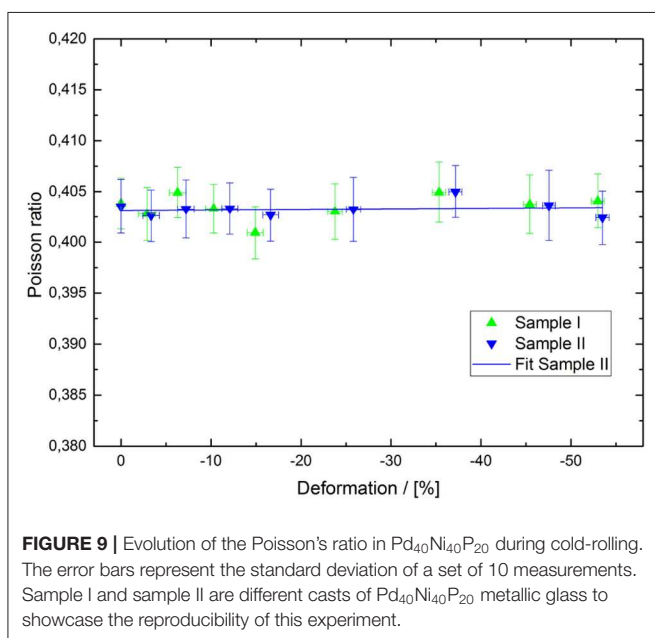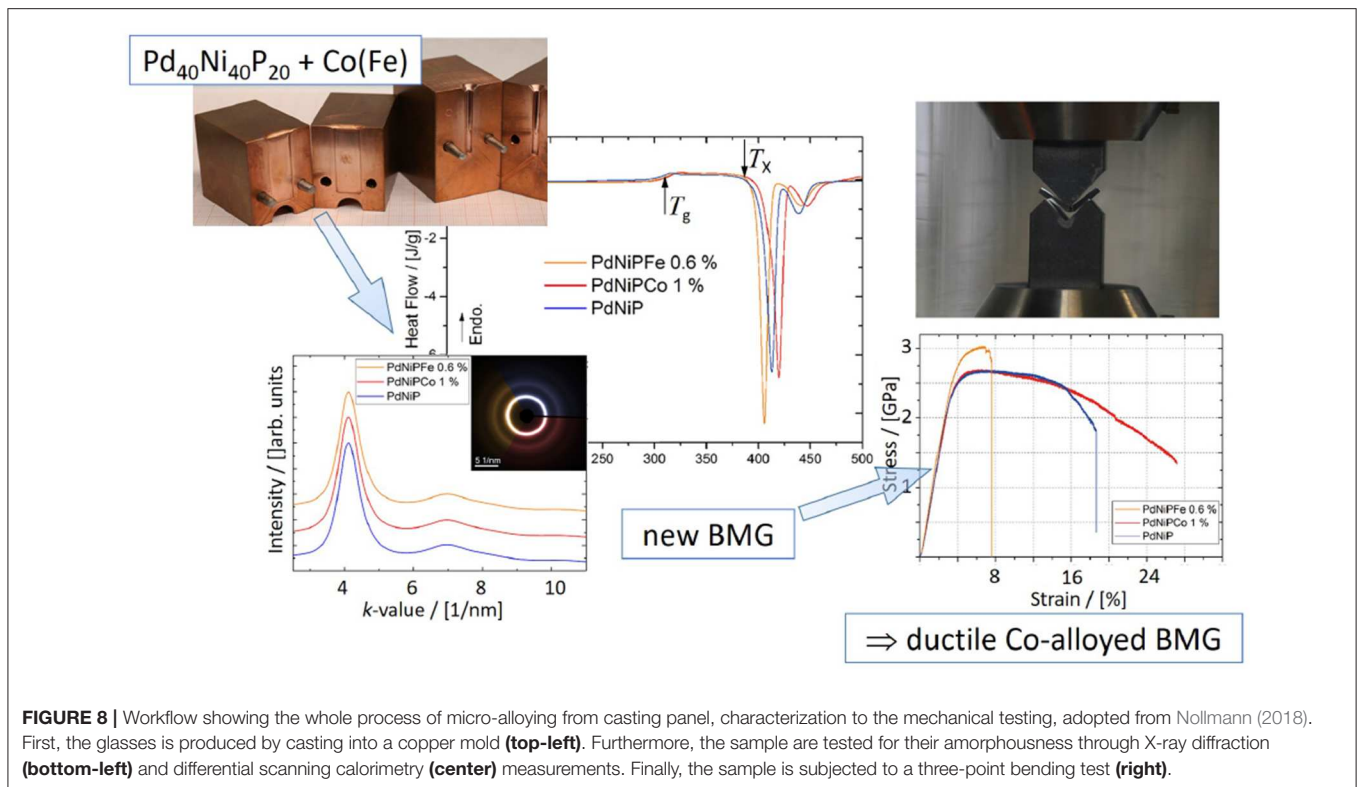
The different shear band types were reported for different glasses, irrespective of their composition (Schroers and Johnson, 2004; Chen et al., 2010). Thus it is important to highlight that in Hubek et al. (2020), an increased heterogeneity of the shear band properties induced by micro-alloying was for the first time reported. Moreover, the tracer diffusion data document the existence of *kinetically different* classes of shear bands. The structural difference between these types has to be elucidated yet. It is probably not just different thickness of the shear bands, especially since the extensive structural and chemical TEM studies (Schmidt et al., 2015) have not revealed an abnormal variation of the shear band thickness which is about 10 nm or less.

One might suggest that porosity could be the origin of the fast diffusion path, but the experiments with the ^{57}Co tracer ruled out this explanation.

6. SUMMARY AND CONCLUSIONS

In this work, we have used a combination of experiment and molecular dynamics (MD) computer simulation to investigate the formation and properties of shear bands in bulk metallic PdNiP glasses under and after mechanical load. While the experiments focussed on the materials properties after shear band formation, in the MD simulation we were aiming at studying the shear band formation during shear on a microscopic level.

An important tool in the experiments is the measurement of tracer diffusion in shear-banded regions. In a cold-rolled

FIGURE 8 | Workflow showing the whole process of micro-alloying from casting panel, characterization to the mechanical testing, adopted from Nollmann (2018). First, the glasses is produced by casting into a copper mold **(top-left)**. Furthermore, the sample are tested for their amorphousness through X-ray diffraction **(bottom-left)** and differential scanning calorimetry **(center)** measurements. Finally, the sample is subjected to a three-point bending test **(right)**.

FIGURE 9 | Evolution of the Poisson's ratio in $Pd_{40}Ni_{40}P_{20}$ during cold-rolling. The error bars represent the standard deviation of a set of 10 measurements. Sample I and sample II are different casts of $Pd_{40}Ni_{40}P_{20}$ metallic glass to showcase the reproducibility of this experiment.

model PdNiP glass, significantly enhanced (akin short-circuit) shear band diffusion is determined at the temperatures at which volume diffusion in as-cast glass is frozen. A cross-over relaxation behavior of shear band diffusion is reported and explained as a counteraction to the redistribution of excess free volume in the deformation-modified volume and in the

shear bands. The Co micro-alloyed glass reveals unambiguously the existence of at least two distinct families of short circuits, namely the "fast" diffusion paths (typically for Co-free PdNiP glasses) and a second type of "ultrafast" paths (with the diffusion coefficients higher by two orders of magnitude). The second path is attributed to a special type of shear bands. Such shear bands are either absent in the Co-free glass or their number density is below the detection limit of the applied radiotracer technique. There is a clear difference between the optically observable primary and secondary shear bands—available in fact in both types of the glassy systems—and the kinetically different shear bands. Co micro-alloying was unambiguously shown to enhance ductility of a model PdNiP glass, whereas addition of Fe or Cu increases brittleness. A correlation of the enhanced ductility, appearance of specific MRO motives and the existence of kinetically specific shear bands upon Co alloying is established. The diffusion enhancement in plastically deformed Co-alloyed glass shows specific response upon annealing below glass transition temperature with a cross-over type of behavior and the different time scales of relaxation for kinetically different types of shear bands.

In the MD simulations, we consider a binary Lennard-Jones model that can be considered as a model for $Ni_{80}P_{20}$. Shear at a constant shear rate is imposed on this system using a planar Couette flow geometry. The sheared glasses show the typical stress-strain relations with an overshoot around a strain of $\gamma = 0.08$, marking the onset of plastic flow. Right after the stress overshoot, prior to the steady state, there is the emergence of inhomogeneous flow patterns. Both vertical and horizontal shear

bands are observed. While the vertical bands lead to a relatively quick approach of the steady state, the horizontal bands are associated with a local potential energy minimum and a slow growth with increasing strain (we note that the width of the shear band increases in a subdiffusive manner; Golkia et al., 2020). The emergence of horizontal shear bands is intimately linked to the level of annealing of the initial undeformed glass state and the the applied strain rate (Golkia et al., 2020). Well-annealed glasses in combination with low shear rates exhibit a high affinity to form horizontal shear bands. This finding indicates why, on the experimental scales, shear banding appears to be a common feature in BMGs.

Another issue that we have addressed in our work is the question whether one can infer the plastic response of BMGs from their elastic properties. The evolution of the Poisson's ratio of $Pd_{40}Ni_{40}P_{20}$ BMG during deformation was measured by ultrasonic measurements revealing no detectable changes. These findings are supported by the MD simulations. Thus, we conclude that the value of the Poisson's ratio cannot be used as an unambiguous criterion of the ductility of any BMG. As the MD simulation indicates, this is also true for other elastic properties Golkia et al.. We propose that the specific changes of MRO parameters and the kinetic response of deformed glasses are key features for adequate description of deformation phenomena both in BMGs as well as in inorganic glasses. The comparison of plastic flow in BMGs to that in inorganic glasses such as silica will be a theme of forthcoming studies.

DATA AVAILABILITY STATEMENT

The raw data supporting the conclusions of this article will be made available by the authors, without undue reservation, to any qualified researcher.

AUTHOR CONTRIBUTIONS

SD, HR, JH, and GW designed the research. RH, SH, FD, MG, GS, SD, and HR performed the research. SD, HR, JH, GW, RH, SH, FD, MG, and GS analyzed the data. SD, HR, JH, and GW wrote the paper.

ACKNOWLEDGMENTS

REFERENCES

Agoritsas, E., and Martens, K. (2017). Non-trivial rheological exponents in sheared yield stress fluids. *Soft Matter* 13:4653. doi: 10.1039/c6sm02702d

Alix-Williams, D. D., and Falk, M. L. (2018). Shear band broadening in simulated glasses. *Phys. Rev. E* 98:053002. doi: 10.1103/PhysRevE.98.053002

Argon, A. S. (1979). Plastic deformation in metallic glasses. *Acta Metallur.* 27:47.

Ashby, M. F., and Greer, A. L. (2006). Metallic glasses as structural materials. *Scrip. Mater.* 54, 321–326. doi: 10.1016/j.scriptamat.2005.09.051

Bartsch, A., Rätzke, K., Meyer, A., and Faupel, F. (2010). Dynamic arrest in multicomponent glass-forming alloys. *Phys. Rev. Lett.* 104:195901. doi: 10.1103/PhysRevLett.104.195901

Binkowski, I., Shrivastav, G. P., Horbach, J., Divinski, S. V., and Wilde, G. (2016). Shear band relaxation in a deformed bulk metallic glass. *Acta Mater.* 109, 330–340. doi: 10.1016/j.actamat.2016.02.061

Bokeloh, J., Divinski, S. V., Reglitz, G., and Wilde, G. (2011). Accelerated diffusion along shear bands in metallic glass. *Phys. Rev. Lett.* 107:235503. doi: 10.1103/PhysRevLett.107.235503

Chattoraj, J., and Lemaître, A. (2013). Elastic signature of flow events in supercooled liquids under shear. *Phys. Rev. Lett.* 111:066001. doi: 10.1103/PhysRevLett.111.066001

Chen, K.-W., and Lin, J.-F. (2010). Investigation of the relationship between primary and secondary shear bands induced by indentation in bulk metallic glasses. *Int. J. Plast.* 26, 1645–1658. doi: 10.1016/j.ijplas.2010.03.003

Chen, N., Martin, L., Luzguine-Luzgin, D. V., and Inoue, A. (2010). Role of alloying additions in glass formation and properties of bulk metallic glasses. *Materials* 3, 5320–5339. doi: 10.3390/ma3125320

Chhabra, R. P., and Richardson, J. F. (2008). *Non-Newtonian Flow and Applied Rheology, 2nd Edn.* Oxford: Elsevier Butterworth-Heinemann.

Dasgupta, R., Hentschel, H. G. E., and Procaccia, I. (2012). Microscopic mechanism of shear bands in amorphous solids. *Phys. Rev. Lett.* 109:255502. doi: 10.1103/PhysRevLett.109.255502

Dasgupta, R., Hentschel, H. G. E., and Procaccia, I. (2013). Yield strain in shear banding amorphous solids. *Phys. Rev. E* 87:022810. doi: 10.1103/PhysRevE.87.022810

Davani, F. A., Hilke, S., Rösner, H., Geisler, D., Gebert, A., and Wilde, G. (2020). What renders bulk metallic glass ductile/brittle? - New insight from the medium-range order. *arXiv [Preprint]. arXiv*:2003.01368.

Duine, P. A., Sietsma, J., and Beukel, A. v. d. (1993). Atomic transport in amorphous $Pd_{40}Ni_{40}P_{20}$ near the glass-transition temperature: Au diffusivity and viscosity. *Phys. Rev. B* 48:6957. doi: 10.1103/PhysRevB.48.6957

Falk, M. L., and Langer, J. S. (1998). Dynamics of viscoplastic deformation in amorphous solids. *Phys. Rev. E* 57:7192. doi: 10.1103/PhysRevE.57.7192

Gendelman, O., Jaiswal, P. K., Procaccia, I., Gupta, B. S., and Zylberg, J. (2015). Shear transformation zones: state determined or protocol dependent? *Europhys. Lett.* 109:16002. doi: 10.1209/0295-5075/109/16002

Gleiter, H. (2013). Nanoglasses: a new kind of noncrystalline materials. *Beilstein J. Nanotechnol.* 4:517. doi: 10.3762/bjnano.4.61

Golkia, M., Shrivastav, G. P., Chaudhuri, P., and Horbach, J. (2020) Flow heterogeneities in supercooled liquids and glasses under shear. *arXiv [Preprint]. arXiv*:2004.02868.

Golkia, M., Shrivastav, G. P., Nollmann, N., Hieronymus-Schmidt, V., Rösner, H., Wilde, G., et al. (2020). preprint.

Harrison, L. G. (1961). Influence of dislocations on diffusion kinetics in solids with particular reference to the alkali halides. *Trans. Faraday Soc.* 57, 1191–1199. doi: 10.1039/tf9615701191

Haruyama, O., and Inoue, A. (2006). Free volume kinetics during sub-T_g structural relaxation of a bulk $Pd_{40}Ni_{40}P_{20}$ metallic glass. *Appl. Phys. Lett.* 88:131906. doi: 10.1063/1.2189833

Hassani, M., Zirdehi, E. M., Kok, K., Schall, P., Fuchs, M., and Varnik, F. (2018). Long-range strain correlations in 3D quiescent glass forming liquids. *Europhys. Lett.* 124:18003. doi: 10.1209/0295-5075/124/18003

Hieronymus-Schmidt, V., Rösner, H., Wilde, G., and Zaccone, A. (2017). Shear banding in metallic glasses described by alignments of Eshelby quadrupoles. *Phys. Rev. B* 95:134111. doi: 10.1103/PhysRevB.95.134111

Hilke, S., Rösner, H., Geissler, D., Gebert, A., Peterlechner, M., and Wilde, G. (2019). The influence of deformation on the medium-range order of a Zr-based bulk metallic glass characterized by variable resolution fluctuation electron microscopy. *Acta Mater.* 171:275–281. doi: 10.1016/j.actamat.2019.04.023

Hubek, R., Seleznev, M., Binkowski, I., Peterlechner, M., Divinski, S. V., and Wilde, G. (2020). Intrinsic heterogeneity of shear banding: hints from diffusion and

relaxation measurements of Co micro-alloyed PdNiP-based glass. *J. Appl. Phys.* 127:115109. doi: 10.1063/1.5142162

Klaumünzer, D., Lazarev, A., Maaß, R., Dalla Torre, F., Vinogradov, A., and Löffler, J. F. (2011). Probing shear-band initiation in metallic glasses. *Phys. Rev. Lett.* 107:185502. doi: 10.1103/PhysRevLett.107.185502

Kob, W., and Andersen, H. C. (1994). Scaling behavior in the β-relaxation regime of a supercooled Lennard-Jones mixture. *Phys. Rev. Lett.* 73, 1376–1379. doi: 10.1103/PhysRevLett.73.1376

Kumar, G., Neibecker, P., Liu, Y. H., and Schroers, J. (2013). Critical fictive temperature for plasticity in metallic glasses. *Nat. Commun.* 4:1536. doi: 10.1038/ncomms2546

Lechner, W., Puff, W., Wilde, G., and Würschum, R. (2010). Vacancy-type defects in amorphous and nanocrystalline Al alloys: variation with preparation route and processing. *Scripta Mater.* 62, 439–442. doi: 10.1016/j.scriptamat.2009.11.037

Lees, A. W., and Edwards, S. F. (1972). The computer study of transport processes under extreme conditions, *J. Phys. C* 5:1921.

Lewandowski, J. J., and Greer, A. L. (2005). Temperature rise at shear bands in metallic glasses. *Nat. Mater.* 5, 15–18. doi: 10.1038/nmat1536

Lewandowski, J. J., Wang, W. H., and Greer, A. L. (1993). Intrinsic plasticity of brittleness of metallic glasses. *Philos. Mag. Lett.* 85, 77–87. doi: 10.1080/09500830500080474

Maaß, R., Samwer, K., Arnold, W., and Volkert, C. A. (2014). A single shear band in a metallic glass: local core and wide soft zone. *Appl. Phys. Lett.* 105:171902. doi: 10.1063/1.4900791

Mitrofanov, Y. P., Peterlechner, M., Binkowski, I., Zadorozhnyy, M. Y., Golovin, I. S., Divinski, S. V., et al. (2015). The impact of elastic and plastic strain on relaxation and crystallization of PdNiP-based bulk metallic glasses. *Acta Mater.* 90:318. doi: 10.1016/j.actamat.2015.03.001

Mitrofanov, Y. P., Peterlechner, M., Divinski, S. V., and Wilde, G. (2014). Impact of plastic deformation and shear band formation on the boson heat capacity peak of a bulk metallic glass. *Phys. Rev. Lett.* 112:135901. doi: 10.1103/PhysRevLett.112.135901

Nollmann, N. (2018). *Plastische Deformation und mechanische Eigenschaften von Palladium-basierten metallischen Gläsern* (Ph.D. thesis). Münster University, Münster, Germany.

Nollmann, N., Binkowski, I., Schmidt, V., Rösner, H., and Wilde, G. (2016). Impact of micro-alloying on the plasticity of Pd-based bulk metallic glasses. *Scripta Mater.* 111, 119–122. doi: 10.1016/j.scriptamat.2015.08.030

Ovarlez, G., Cohen-Addad, S. Krishan, K., Goyon, J., and Coussot, P. (2013). On the existence of a simple yield stress fluid behavior. *J. Non-Newton. Fluid Mech.* 193, 68–79. doi: 10.1016/j.jnnfm.2012.06.009

Ozawa, M., Berthier, L., Biroli, G., Rosso, A., and Tarjus, G. (2018). Random critical point separates brittle and ductile yielding transitions in amorphous materials. *Proc. Natl. Acad. Sci. U.S.A.* 115, 6656–6661. doi: 10.1073/pnas.1806156115

Parmar, A. D. S., Kumar, S., and Sastry, S. (2019). Strain localization above the yielding pont in cyclically deformed glasses. *Phys. Rev. X* 9:021018. doi: 10.1103/PhysRevX.9.021018

Paul, A., Laurila, T., Vuorinen, V., and Divinski, S. V. (2014). *Thermodynamics, Diffusion and the Kirkendall Effect in Solids* . Heidelberg: Springer.

Plimpton, S. (1995). Fast parallel algorithms for short-range molecular dynamics. *J. Comput. Phys.* 117, 1–19. doi: 10.1006/jcph.1995.1039

Radek, M., Tenberge, J.-G., Hilke, S., Wilde, G. and Peterlechner, M. S (2018). TEMclA multi-GPU multislice algorithm for simulation of large structure and imaging parameter series. *Ultramicroscopy* 188, 24–30. doi: 10.1016/j.ultramic.2018.02.004

Radić, D., Hilke, S., Peterlechner, M., Posselt, M., and Bracht, H. (2019). Fluctuation electron microscopy on silicon amorphized at varying self ion-implantation conditions. *J. Appl. Phys.* 126:095707. doi: 10.1063/1.5107494

Rösner, H., Peterlechner, M., Kübel, C., Schmidt, V., and Wilde, G. (2014). Density changes in shear bands of a metallic glass determined by correlative analytical transmission electron microscopy. *Ultramicroscopy* 142, 1–9. doi: 10.1016/j.ultramic.2014.03.006

Schmidt, V., Rösner, H., Peterlechner, M., Wilde, G., and Voyles, P. M. (2015). Quantitative measurement of density in a shear band of metallic glass monitored along its propagation direction. *Phys. Rev. Lett.* 115:035501. doi: 10.1103/PhysRevLett.115.035501

Schroers, J., and Johnson, W. L. (2004). Ductile bulk metallic glass. *Phys. Rev. Lett.* 93:255506. doi: 10.1103/PhysRevLett.93.255506

Shao, H., Xu, Y., Shi, B., Yu, C., Hahn, H., Gleiter, H., et al. (2013). High density of shear bands and enhanced free volume induced in $Zr_{70}Cu_{20}Ni_{10}$ metallic glass by high-energy ball milling. *J. Alloys Compounds* 548, 77–81. doi: 10.1016/j.jallcom.2012.08.132

Shrivastav, G. P., Chaudhuri, P., and Horbach, J. (2016a). Heterogeneous dynamics during yielding of glasses: effect of aging. *J. Rheol.* 60, 835–847. doi: 10.1122/1.4959967

Shrivastav, G. P., Chaudhuri, P., and Horbach, J. (2016b). Yielding of glass under shear: a directed percolation transition precedes shear-band formation. *Phys. Rev. E* 94:042605. doi: 10.1103/PhysRevE.94.042605

Soddemann, T., Dünweg, B., and Kremer, K. (2003). Dissipative particle dynamics: a useful thermostat for equilibrium and nonequilibrium molecular dynamics simulations. *Phys. Rev. E* 68:046702. doi: 10.1103/PhysRevE.68.046702

Taub, A. I., and Spaepen, F. (1980). The kinetics of structural relaxation of a metallic glass. *Acta Metallur.* 28, 1781–1788. doi: 10.1016/0001-6160(80)90031-0

Tool, A. Q., and Eichlin, C. G. (1931). Variations caused in heating curves of glass by heat treatment. *J. Am. Ceram. Soc.* 14, 276–308. doi: 10.1111/j.1151-2916.1931.tb16602.x

Treacy, M. M. J., and Gibson, J. M. (1996). Variable coherence microscopy: a rich source of structural information from disordered materials. *Acta Crystallogr. Sect. A* 52:212.

Treacy, M. M. J., Gibson, J. M., Fan, L., Paterson, D. J., and McNulty, I. (2005). Fluctuation microscopy: a probe of medium range order. *Rep. Prog. Phys.* 68:2899. doi: 10.1088/0034-4885/68/12/R06

Voyles, P., and Muller, D. (2002). Fluctuation microscopy in the STEM. *Ultramicroscopy* 93, 147–159. doi: 10.1016/S0304-3991(02)00155-9

Wilde, G., Görler, G. P., Willnecker, R., and Fecht, H. J. (2000). Calorimetric thermomechanical and rheological characterizations of bulk metallic glassforming: $Pd_{40}Ni_{40}P_{20}$, *J. Appl. Phys.* 87:1141. doi: 10.1063/1.371991

Wilde, G., Sebright, J. L., and Perepezko, J. H. (2006). Bulk liquid undercooling and nucleation in gold. *Acta Mater.* 54, 4759–4769. doi: 10.1016/j.actamat.2006.06.007

Zausch, J., and Horbach, J. (2009). The build-up and relaxation of stresses in a glassforming soft-sphere mixture under shear: a computer simulation study. *Europhys. Lett.* 88:60001. doi: 10.1209/0295-5075/88/60001

Zausch, J., Horbach, J., Laurati, M., Egelhaaf, S. U., Brader, J. M., Voigtmann, T., et al. (2008). From equilibrium to steady state: the transient dynamics of colloidal liquids under shear. *J. Phys.: Condens. Matter* 20:404120. doi: 10.1088/0953-8984/20/40/404210